AIAA JOURNAL
Vol. 34, No. 4, April 1996

Comparison of Temporal and Spatial Direct Numerical Simulation of Compressible Boundary-Layer Transition

Yan Guo,* Leonhard Kleiser,† and Nikolaus A. Adams‡
Swiss Federal Institute of Technology, CH-8092 Zürich, Switzerland

Two models are used in the direct numerical simulation of transitional boundary-layer flows, the spatial model and the temporal model. The spatial approach is the closest realization of a transition experiment but is significantly more expensive than the temporal approach, which employs a local parallel flow assumption in its formulation. Because of the parallel flow assumption, a temporal approach cannot take into account the nonparallel effects of boundary-layer flows properly. The consequence of this defect has never been addressed adequately. In this study, the results from various temporal approaches are compared extensively to those obtained by our two newly developed spatial direct numerical simulation codes for nonlinear subharmonic transition and oblique wave breakdown at Mach numbers 1.6 and 4.5. A recently developed new temporal approach that can include some nonparallel effects in the computation is also introduced. The use of our new formulation is essential in obtaining quantitative agreement with the spatial approach at high Mach numbers, whereas the standard temporal approach does not give satisfactory results.

Nomenclature

c_T	= frame speed
E	= total energy
k	= wave number
M_∞	= freestream Mach number
p	= pressure
Re	= Reynolds number
T	= temperature
u, v, w	= velocity components
α	= streamwise wave number
β	= spanwise wave number
κ	= ratio of specific heats
ρ	= density
ω	= angular frequency

I. Introduction

RECENTLY with the vast increase of computing power, direct numerical simulation (DNS) of transitional boundary-layer flows has become a valuable tool providing databases for modeling transitional and turbulent flows. This is especially important for high-speed boundary-layer flows, where experimental approaches have encountered enormous difficulties in obtaining detailed information about the transition process and turbulent quantities. In this study, our recent efforts toward DNS of transition in compressible boundary-layer flows are outlined. Attention is given to the comparison of the two DNS approaches, the spatial and the temporal DNS.

In the DNS of a transitional boundary layer, the computational domain is usually a truncation of the physical domain, as is shown by the dashed lines in Fig. 1. We designate x as the streamwise direction, y as the spanwise direction, and z as the wall-normal direction. The boundary-layer thickness δ_0 increases in the streamwise direction. Currently, two approaches are used in DNS: spatial DNS (SDNS) and temporal DNS (TDNS). In an SDNS, inflow boundary conditions are prescribed, and the flow develops spatially in the streamwise direction. This is the closest numerical realization of a transition experiment. Because of the difficulties in finding appropriate inflow and outflow boundary conditions at the domain truncation planes, the computational box is usually quite long in the streamwise direction (typically several dozen wavelengths of the primary instability waves at high Mach number). This requires very large computing resources. So far, except for a few cases,[1,2] SDNS has been limited mainly to the earlier stages of the transition.[3–6]

Because the development of boundary layers in the streamwise direction is rather slow in comparison to that of an instability wave, a local parallel flow assumption is often made, and the inflow/outflow boundary conditions are replaced by periodic boundary conditions. This is a TDNS approach (compare Ref. 7). Because the flow is assumed to be periodic in the streamwise direction, the computational box can be very short (one or a few primary instability wavelengths) and Fourier spectral schemes can be used in this direction. Thus, the TDNS is a highly efficient approach. Using this approach, the DNS of a complete subharmonic transition process from laminar to turbulent boundary layer at $M_\infty = 4.5$ has recently been performed by Dinavahi et al.[8] and Guo et al.[9] For other recent work on compressible boundary-layer transition, readers are referred to Refs. 10–16. To study the effect of a growing boundary layer on instability waves and transition, the computational box can be moved downstream at some speed c_T, which is usually chosen to be close to the group speed of the instability waves, and the boundary-layer grows in time (compare Spalart and Yang[17]). For convenience, we refer to Spalart and Yang's approach[17] as the standard TDNS approach in this study.

One drawback of the TDNS is its inability to take into account the nonparallel effects resulting from the use of the parallel flow assumption. To our knowledge, the accuracy of the TDNS for nonparallel boundary-layer flows has not been adequately addressed. No thorough comparison has been carried out between TDNS and

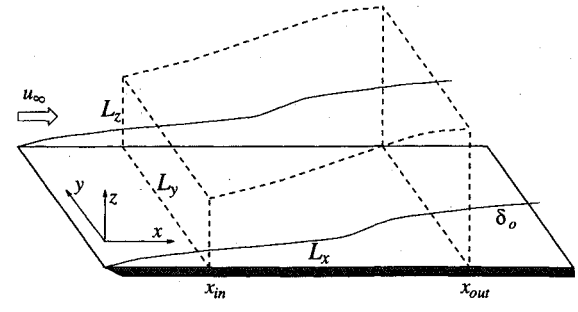

Fig. 1 Sketch of the computational domain of a growing boundary layer.

Received June 14, 1994; presented as Paper 94-2371 at the AIAA 25th Fluid Dynamics, Plasmadynamics, and Lasers Conference, Colorado Springs, CO, June 20–23, 1994; revision received Dec. 9, 1994; accepted for publication Dec. 12, 1994.

*Postdoctoral Assistant, Institute of Fluid Dynamics; currently Research Scientist, High Technology Corp., Hampton, VA 23666. Member AIAA.
†Professor, Institute of Fluid Dynamics. Member AIAA.
‡Postdoctoral Assistant; currently Research Scientist, High Technology Corp., Hampton, VA 23666.

SDNS for these flows. Our recent experience with the TDNS has shown that a direct application of the standard parallel flow formulation to supersonic/hypersonic boundary layers is not satisfactory. Considerable discrepancies were found in the growth rates of the instability waves between this approach and other sources, e.g., parabolized stability equations[18] (PSE) and SDNS. Thus, there is a need to improve the effectiveness of the TDNS for nonparallel flows.

In Guo et al.,[19] we have developed a new temporal approach that can model some nonparallel effects of boundary-layer flows. Initial comparison between this approach[19] and PSE[18] or SDNS[4,6,19] has shown a significant improvement of this approach over the standard TDNS. But because of lack of our own SDNS results for nonlinear stages of transition at high Mach numbers, the comparison was limited to either linear stages of transition or weakly nonlinear stages at low Mach numbers. Recently, we developed two SDNS codes, which make possible the quantitative comparison between various TDNS and SDNS approaches for nonlinear stages of transition at various Mach numbers. In the present study, in Sec. II we first briefly outline the new TDNS approach developed by Guo et al.[19] Features of our two SDNS codes are reported in Sec. III. In Sec. IV we present extensive comparison between various TDNS and SDNS approaches for nonlinear stages of transition at Mach numbers 1.6 and 4.5. Discussions and concluding remarks are given in Sec. V.

II. Modeling Nonparallel Effects in Temporal DNS

In a TDNS, one primary concern is the use of periodic inflow and outflow boundary conditions, which allows us to employ Fourier spectral schemes (and a small computational box) in the streamwise direction. There is no need to invoke a parallel flow assumption, which originated from the early linear stability theory for boundary-layer flows (compare Lin[20]). After identifying this limitation of a TDNS approach, we have developed an approach[19] that allows us to model nonparallel effects in the framework of a TDNS. The basic idea of this approach is as follows. Suppose we can approximate a nonparallel flowfield $\boldsymbol{u}(x, y, z, t)$ by a truncated series

$$\boldsymbol{u}(x, y, z, t) \approx \boldsymbol{u}_0 + \boldsymbol{u}_1\epsilon(x)^1 + \boldsymbol{u}_2\epsilon(x)^2 + \cdots + \boldsymbol{u}_n\epsilon(x)^n \qquad (1)$$

where $\boldsymbol{u}_i$ [$= \boldsymbol{u}_i(x, y, z, t), i = 0, 1, \ldots, n$] are periodic functions in the x and y directions and $\epsilon(x)$ is related to the slow variation of the flow in the x direction. Then we can reformulate the governing equations in the function space ϵ^i ($i = 0, 1, \ldots, n$) by substituting Eq. (1) into the Navier–Stokes equations, yielding one set of equations for each i. The unknowns in these equation sets are $\boldsymbol{u}_i$ ($i = 0, 1, \ldots, n$), and conceptually a conventional TDNS code can be modified to solve these sets of equations. In Guo et al.[19] we have shown that expansion (1) exists for transitional boundary-layer flows when the wavelengths of the instability waves under consideration are not too long and their frequencies are not too small. For more details of this approach refer to Guo et al.[19] In this study, we refer to this approach as the extended TDNS approach.

Because of the complexity of this approach for a compressible boundary layer, only the first set of equations in the space $\epsilon(x)^0$ is considered, which has the form

$$\frac{\partial \boldsymbol{U}}{\partial t} = \frac{\partial \boldsymbol{E}}{\partial x} + \frac{\partial \boldsymbol{F}}{\partial y} + \frac{\partial \boldsymbol{G}}{\partial z} + \boldsymbol{Z}_1 + \boldsymbol{Z}_2 + \boldsymbol{Z}_3 \qquad (2)$$

The vector $\boldsymbol{U}$ is the solution vector defined by $\boldsymbol{U} = (\rho, \rho u, \rho v, \rho w, E)^T$. The total energy E is defined by $E = p/(\kappa - 1) + \rho(u^2+v^2+w^2)/2$. Here the freestream quantities are used to nondimensionalize Eq. (2). The reference length is the displacement thickness δ_1^* of the undisturbed laminar basic flow at the reference position given by the respective Reynolds number Re. The pressure p is related to the temperature T by a perfect-gas law, $p\kappa M_\infty = \rho T$. Sutherland's law is used for the viscosity calculation. The vectors $\boldsymbol{E}$, $\boldsymbol{F}$, and $\boldsymbol{G}$ are the flux vectors in the streamwise, spanwise, and wall-normal directions, respectively. They resemble the standard compressible Navier–Stokes equations (in conservative form). The additional terms $\boldsymbol{Z}_1, \boldsymbol{Z}_2$, and $\boldsymbol{Z}_3$ come from our new formulation and are fully explained in Guo et al.[19]

The TDNS code developed by Adams[10] has been modified to solve Eq. (2). It employs a Fourier collocation method in the streamwise and spanwise directions, and a sixth-order compact central finite difference (Padé) scheme in the wall-normal direction. No-slip conditions for the velocity and isothermal conditions for the temperature are used at the wall. At the upper truncation plane, nonreflecting boundary conditions are implemented. The solution is advanced in time explicitly by a third-order Runge–Kutta scheme.

III. Spatial DNS

To quantify the performance of our extended TDNS approach for nonparallel boundary-layer flows, we have recently developed two SDNS codes.[21,22] In this section, we outline some basic features of these two codes. Attention is given to the correct specification of the inflow and outflow boundary conditions, since this issue is especially important for high-order schemes where the numerical dissipation is very low. Improper treatments of inflow/outflow conditions usually lead to unacceptable wave reflection problems.

A. Finite Difference Approach

Our first code[21] employs a sixth-order Padé scheme in the streamwise and wall-normal directions. A Fourier collocation scheme is used in the spanwise direction, since the flow can be assumed to be periodic in this direction. Time advancement is achieved by a low-storage third-order Runge–Kutta scheme. Grid stretching is used in both the streamwise and wall-normal directions. The wall conditions and the boundary conditions at the upper truncation plane are the same as those used in our TDNS codes.

A characteristic inflow boundary condition is employed at the inflow boundary. To enforce prescribed disturbances with large amplitudes at the inflow boundary, the flowfield is first decomposed into three parts: the given laminar basic flow, the prescribed perturbation, and the remaining part. We refer to this part as the residual disturbance. At the supersonic section of the inflow boundary, the residual disturbance part can be assumed to be zero, and all of the variables of the basic flow and the prescribed perturbation are imposed. At the subsonic section, the basic flow and prescribed perturbation are imposed while a characteristic boundary condition[23] is applied to the residual disturbance part, which allows the out-going waves to pass the boundary with minimum reflection. This splitting is quite important, since it allows characteristic boundary conditions to be applied to the residual disturbance only. The advantage of this inflow treatment over the one in Poinsot and Lele[23] is that this treatment allows us to correctly enforce the prescribed perturbation at the inflow boundary without any visible wave reflection.

At the outflow boundary, three treatments have been implemented: characteristic-based boundary conditions (compare Ref. 23), a buffer domain approach (compare Ref. 24), and a sponge layer approach (i.e., a damping function approach; compare Refs. 25–27). The effectiveness of these boundary treatments is tested by simulating two- and three-dimensional instability waves and comparing the results with those of linear stability theory[28] (LST), PSE,[18,24] and other SDNS codes.[22,24]

Figure 2 shows the growth rates of a second-mode wave (Mack mode[29]) in a parallel basic flow ($M_\infty = 4.5$ and $T_\infty = 61.15$ K), obtained with different outflow treatments. We choose $Re = 8000$ as the reference Reynolds number and the corresponding displacement thickness δ_1^* as the reference length. The similarity solution of the compressible boundary-layer equations[10] at $x = 100$ is used as the parallel basic flow in the computation. The streamwise wave number of the second mode is $\alpha = 1.942$, and the frequency is $\omega = 1.766$. The spatial growth rate from LST is 2.504×10^{-2}. To study the performance of the outflow treatments, we use a rather high resolution in the streamwise direction, 20 points per wavelength. The number of time steps per period is around 150. Note that the growth rate is one of the most sensitive indicators of any numerical error, inflow/outflow boundary coupling, or wave reflection. The local growth rate is calculated (using a central difference scheme) from the local maximum of the quantity $\tilde{u}_{k_y}(x, z, t) - \delta_{0k_y}\bar{u}$ taken at $z = 0.374$ within one period. Here, $\delta_{0k_y} = 0$ for $k_y \neq 0$, $\bar{u}$ is the streamwise velocity component of the basic flow, and $\tilde{u}_{k_y}(x, z, t)$ is the spanwise Fourier mode with the spanwise wave number k_y.

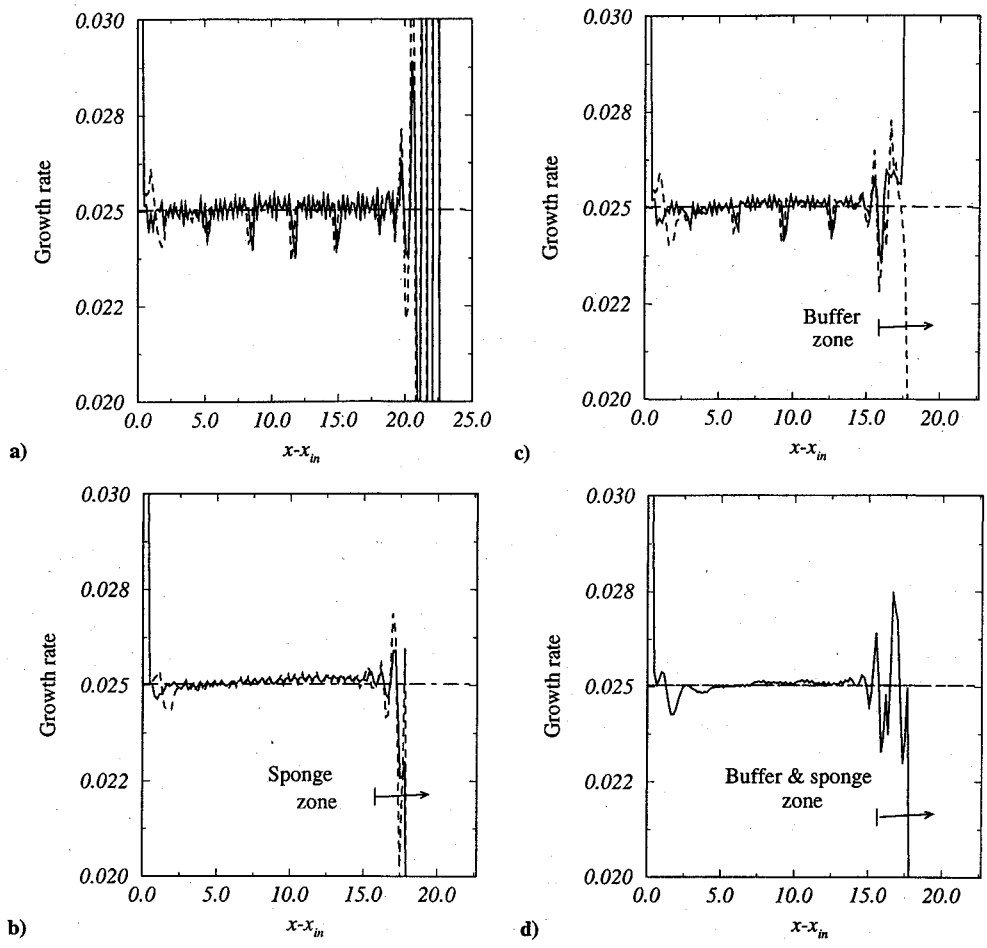

Fig. 2 Spatial growth rates of a two-dimensional wave in a parallel mean flow calculated with different outflow treatments: a) characteristic boundary conditions, b) characteristic boundary conditions and sponge layer, c) buffer domain, and d) buffer domain and sponge layer. ——, energy; – – –, $u|_{z=0.37355}$; and –·–, LST.

The energy growth rate is calculated in a similar way but from the kinetic energy contained in the spanwise Fourier mode:

$$E_{k_y}(x,t) = \int_0^{z_{\max}} \bar{\rho}(z)\left|\tilde{u}_{k_y}(x,z,t) - \delta_{0k_y}\bar{u}\right|^2 \mathrm{d}z \tag{3}$$

The local growth rates calculated from $\tilde{\rho}_{k_y}(x,z,t)$, $\tilde{w}_{k_y}(x,z,t)$, and $\tilde{T}_{k_y}(x,z,t)$ are quite similar to those of $\tilde{u}_{k_y}(x,z,t)$ and, therefore, are not shown in Fig. 2.

In all cases, there are small transients shortly after x_{in}. This is expected since the eigensolutions from LST are not solved in the same manner as in our SDNS (e.g., different formulations, numerical methods, and grid points). Farther downstream, the growth rate approaches that of LST. Near the outflow region, the growth rate experiences rather large fluctuations. These are limited to the outflow region, and they do not affect the solution upstream.

In Figs. 2a and 2c, there are small pulses traveling downstream throughout the entire domain. Our further study confirms that these pulses are a result of the inflow/outflow boundary coupling. In the case of characteristic outflow boundary conditions, the coupling is always present, and the amplitudes of the pulses depend on the number of grids per wavelength. The more grid points per wavelength, the smaller the pulses are. In the case of the buffer domain approach, the pulses also depend on the design of the buffer domain. This confirms the observations of Joslin et al.[30] and Liu and Liu.[31] However, how the buffer domain affects the results has not been extensively studied, due to the rather high computational cost.

When a sponge layer is added to the outflow region, the results (shown in Figs. 2b and 2d) are significantly improved. The small pulses present in Figs. 2a and 2c are no longer observed. The eigenvalues match those of LST up to five digits in both cases. It appears that two outflow treatments perform best: characteristic boundary conditions combined with a sponge layer and a buffer domain approach plus a sponge layer. The use of the sponge layer is indispensable. These treatments are better than those that use only characteristic conditions[23] or the buffer domain approach alone.[24]

B. Spatial Window Approach

In almost all SDNS approaches, the computational box is a simple truncation from the physical domain. In a sense, this procedure is equivalent to using a rectangular window function defined by

$$w(x) = \begin{cases} 1 & x \in [x_{\text{in}}, x_{\text{out}}] \\ 0 & \text{otherwise} \end{cases} \tag{4}$$

to sample the flowfield in the streamwise direction. In a more general case, a window function of the form

$$w(x) = \begin{cases} w(x) & x \in [x_{\text{in}}, x_{\text{out}}] \\ 0 & \text{otherwise} \end{cases} \tag{5}$$

can be used. Here $w(x)$ is a smooth function in $[x_{\text{in}}, x_{\text{out}}]$. If the window function is applied, the governing equations in the computational domain take the following form:

$$\frac{\partial w\boldsymbol{U}}{\partial t} = \frac{\partial w\boldsymbol{E}}{\partial x} + \frac{\partial w\boldsymbol{F}}{\partial y} + \frac{\partial w\boldsymbol{G}}{\partial z} + w\boldsymbol{Z} - \frac{\mathrm{d}w}{\mathrm{d}x}\boldsymbol{E} \tag{6}$$

where the terms $\boldsymbol{E}$, $\boldsymbol{F}$, and $\boldsymbol{G}$ have definitions similar to those in Eq. (2). The term $\boldsymbol{Z}$ is the forcing term used to enforce a prescribed laminar basic flow (compare Guo et al.[22]). When a rectangular window function, i.e., $w(x) = 1$, is used, the standard Navier–Stokes equations are recovered from Eq. (6).

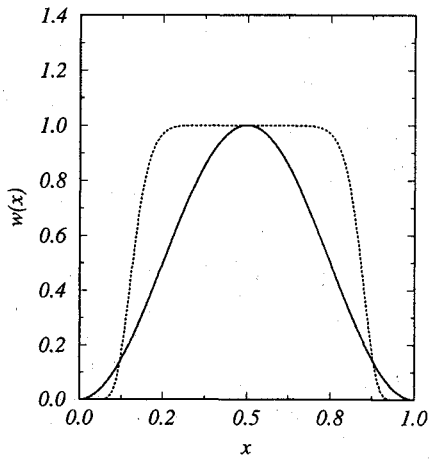

Fig. 3 Hanning window w_H and an exponential window w_e: ——, w_H and ·····, w_e.

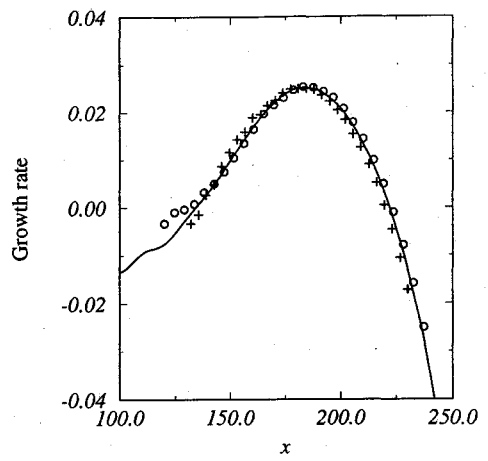

Fig. 4 Spatial growth rates of a linear second-mode wave at M_∞ = 4.5, obtained with different approaches: ○, FD approach; +, window approach; and ——, PSE.

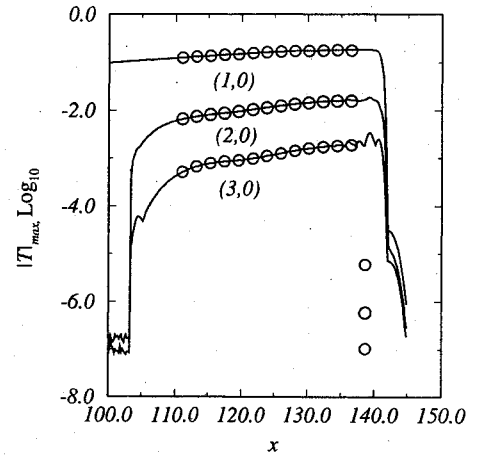

Fig. 5 Temperature amplitude maxima of a nonlinear second-mode wave as a function of the streamwise distance; only the primary wave and its first two harmonics are shown: ○, FD approach and ——, window approach.

It can be shown that Eq. (6) can be solved efficiently by Fourier spectral methods in the streamwise direction if the window function $w(x)$ is properly designed. Motivated by this observation, we have developed a spatial window approach, which solves Eq. (6) using a modified TDNS code.[22] It can be shown that the accuracy of such an approach depends only on the window function $w(x)$ itself, and window functions that yield exponential accuracy can be designed. Figure 3 shows such a window defined by $w_e(x) = 10^{-a^n(2x-1)^n}$, $x \in [0, 1]$ with $a = 1.3$ and $n = 10$. We refer to this window as an exponential window, since its spectrum decays exponentially. The value of $\epsilon = w_e(0) = w_e(1)$ is referred to as the window truncation error. For the exponential window in Fig. 3, $\epsilon = 1.63739 \times 10^{-14}$. Also shown in the figure is a Hanning window of the form $w_H(x) = 0.5\,[1 - \cos(2\pi x)]$, $x \in [0, 1]$. This window has been widely used in digital signal processing for many years.[32,33]

The use of a window function raises some special issues. For example, because of the nonlinearity in the flux terms and the last term in Eq. (6), the vector $\boldsymbol{U}$ is required explicitly at each Runge–Kutta intermediate step. This requires the recovery of $\boldsymbol{U}$ from $w(x)\boldsymbol{U}$. We refer to this process as dewindowing. For any window function that gives exponential accuracy, the information about $\boldsymbol{U}$ cannot be recovered numerically from $w(x)\boldsymbol{U}$ in the neighborhood of x_{in} and x_{out}, since $w(x) \to 0$ at x_{in} and x_{out}. We denote these two regions as $[x_{\text{in}}, x_{\text{in}}^w)$ and $(x_{\text{out}}^w, x_{\text{out}}]$. In the inflow region $[x_{\text{in}}, x_{\text{in}}^w)$, the prescribed disturbance can be used for $\boldsymbol{U}$. In the outflow region $(x_{\text{out}}^w, x_{\text{out}}]$, $\boldsymbol{U}$ is unknown and special treatments must be employed. In Guo et al.,[22] a smooth function is used to reconstruct $\boldsymbol{U}$ from $w(x)\boldsymbol{U}$. Together with a sponge layer in the outflow region this approach has been shown to perform satisfactorily, with no visible inflow/outflow boundary wave reflection. Note that in the useful domain $[x_{\text{in}}^w, x_{\text{out}}^w]$, the window function $w(x)$ is not required to be 1. Also any type of grid stretching in the streamwise direction is allowed, which is considered to be important in the SDNS of boundary-layer transition.[5]

C. Validation of Spatial DNS Codes

Figure 4 shows the spatial growth rates of a linear second-mode wave with $\alpha = 2.0625$ and $\omega = 1.836$ at $M_\infty = 4.5$, $T_\infty = 123$ K, $\kappa = 1.4$, and $Pr = 0.72$. The reference Reynolds number is $Re = 12{,}000$. An eigensolution from LST is used as the disturbance in the inflow region. The magnitude of the disturbance at x_{in} is around 1.0×10^{-4}. In the computation of the window approach, the resolution is 10 grid points per wavelength in the x direction and 121 points in the z direction. An exponential window function with $n = 10$ and $a = 1.258$ ($\epsilon = 1.18376 \times 10^{-10}$) is used. In the computation of the finite difference approach, the resolution is 14 points per wavelength in the x direction and 121 in the z direction. Also given in Fig. 4 are the results obtained by Bertolotti (private communication, 1993), using a PSE approach. The results from the three different approaches agree with each other very well, considering that the growth rate is rather sensitive to any numerical error. Excellent agreement is also found in the amplitude functions of velocity components and temperature.

We have done some numerical tests of the accuracy of the two codes. For the FD approach, we find that it is necessary to use 12 points per wavelength in the x direction to resolve a weakly amplified (or damped) wave. This is in agreement with the experience reported by Pruett et al.[5] on a sixth-order Padé scheme. In the window approach, we find that 7 points per wavelength already give satisfactory results. Generally, the window code needs 15% more computation time per grid point than the FD code. Thus, we can conclude that our unconventional window approach is at least as competitive as the sixth-order Padé scheme.

In our second test, a nonlinear two-dimensional second-mode wave with $\omega = 1.76$ is computed. The flow parameters here are similar to those in Fig. 2, except that the amplitude of the streamwise velocity of the two-dimensional wave is about 1% of the freestream velocity, and the basic flow is nonparallel. To make the comparison between the two SDNS codes, the computation of the nonlinear second mode was first carried out using the window approach. It used 18.5 grid points per wavelength in the streamwise direction and 161 grid points in the wall-normal direction. Then the flow quantities sampled at $x = 111$ were used as the inflow conditions in the FD approach. The resolution used in the FD approach is 32 grid points per wavelength in the x direction and 161 grid points in the z direction. Figure 5 shows the streamwise evolution of the temperature maxima of the primary wave (1, 0) and its first two harmonics. According to our accuracy tests, the primary wave and its first two harmonics should be well resolved in the window approach. In the FD approach, the primary wave and its first harmonic are well resolved, and the second harmonic (3, 0) is marginally resolved. In Fig. 5, we can see that the agreement between the two

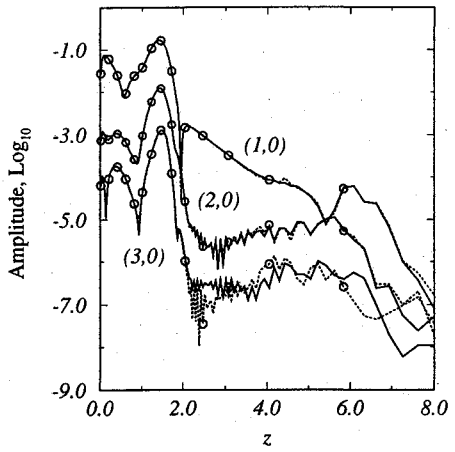

Fig. 6 Temperature amplitude functions of the nonlinear second mode in Fig. 5 at $x = 126.191$ on a logarithmic scale: ○, FD approach and ——, window approach.

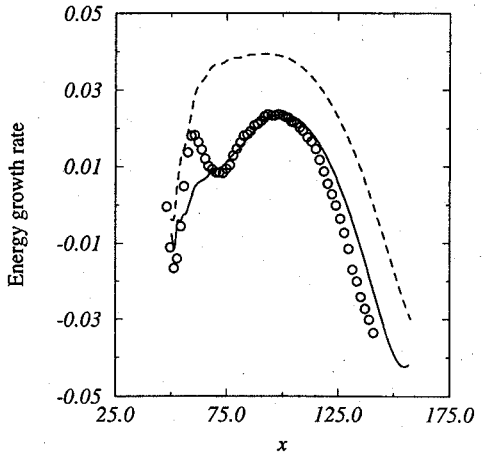

Fig. 7 Spatial growth rates defined by kinetic energy for a linear second mode at $M_\infty = 4.5$: ——, extended TDNS; – – –, standard TDNS; and ○, SDNS.

codes is excellent also in this nonlinear test case. The corresponding amplitude functions at $x = 126.191$ are shown in Fig. 6. Again very good agreement between these two codes is observed.

IV. Numerical Results

A. Linear Waves

Having developed both TDNS and SDNS tools, we are ready to carry out a comparison study between TDNS and SDNS. Figure 7 shows the spatial growth rates obtained by our TDNS and SDNS codes for a linear second mode at $M_\infty = 4.5$. The flow parameters are similar to those in Fig. 5. A similarity solution of the compressible boundary-layer equations is used as the laminar basic flow in all computations. In the SDNS, the frequency of the second mode is $\omega = 1.76$, and the window approach is used. In the extended TDNS, the streamwise wave number is $\alpha = 1.942$, and the frame speed is $c_T = 0.815$, which is the average group velocity of the second mode. We can see that after the initial transient the results from the extended TDNS are quite close to those from SDNS. The results from the standard TDNS are unacceptable. More examples of linear two- and three-dimensional waves at different Mach numbers can be found in Guo et al.[19] In the present study, we concentrate on the computations of the nonlinear stage of transition.

B. Oblique Wave Breakdown at $M_\infty = 4.5$

It has been shown that at high Mach number ($M_\infty > 3$), the transition toward turbulence may take two paths: subharmonic resonance transition and oblique wave breakdown (compare Adams and Kleiser[11]). The first route is the result of a secondary instability mechanism of the two-dimensional second-mode wave, which becomes most unstable at high Mach number. Since the instability

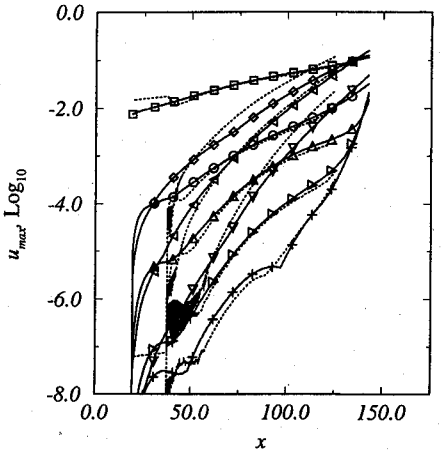

Fig. 8 Maxima of the amplitude functions of the leading modes in a logarithmic scale, obtained by the extended TDNS and SDNS, spatial window approach: ○, (2,0); □, (1,1); ◇, (0,2); △, (3,1); ◁, (1,3); ▽, (0,4); ▷, (4,0); +, (4,4); and ···, SDNS.

domain of the second-mode waves is rather narrow, the most unstable first-mode waves, which are oblique waves, may still have larger growth, and the weakly nonlinear interaction among these oblique waves may lead to the transition. The transition of this type is referred to as an oblique wave breakdown (compare Thumm et al.[6]). In this section, we first investigate the oblique wave breakdown route at $M_\infty = 4.5$. The flow parameters are similar to those in Adams and Kleiser[11]: $M_\infty = 4.5$, $T_\infty = 61.15$ K, $Re = 10{,}000$, and $Pr = 0.7$. In the computations of both SDNS and TDNS, a pair of oblique waves are used to disturb the laminar basic flow. The frequency of the oblique wave is $\omega = 0.3878$. It has a spanwise wave number of $\beta = 0.83$ (oblique angle $\psi = 60$ deg). In the extended TDNS, the streamwise wave number is chosen to be $\alpha = 0.48$. The frame speed is $c_T = 0.82$, which is the average group velocity of the oblique waves.

Figure 8 shows the streamwise development of the leading modes. In the SDNS, the amplitude of the streamwise velocity component of the oblique waves in the inflow region is 1.5% of the freestream velocity, and the spatial window approach is used. In the TDNS, the initial amplitudes of the oblique waves are adjusted to match those in the SDNS. It can be seen that except for the spanwise modes (0, 2) and (0, 4), all of the modes from the extended TDNS agree very well with those from the SDNS when $x > 50$. In $x < 50$, the two approaches have different transients, which lead to slightly different solutions. The relative large discrepancies in modes (0, 2) and (0, 4) may be a result of the fact that the frame speed in the TDNS is significantly larger than the group velocities of these spanwise modes, which are typically in the range of 0.4–0.6. Thus, the spatial growth of these spanwise modes is underestimated in the TDNS. More discussion on the treatment of spanwise modes in the TDNS can be found in Guo and Adams.[34]

The comparison between our two SDNS codes is shown in Fig. 9. Note that the initial amplitudes of the primary oblique waves are not the same in the two SDNS codes. This difference is translated into discrepancies between the results of the two codes, especially in the higher modes. Note that the transition process is very sensitive to the initial amplitude of mode (1, 1). One way to obtain a good comparison is to use the solution from one code as the inflow disturbance in the other code, as has been done in Fig. 5. Since this process is rather tedious, we did not pursue this approach here.

Figure 10 shows the results from the standard TDNS approach, in comparison with those from the window approach. It can be seen that the growth pattern of the leading modes given by the standard TDNS approach is quite different from that of the SDNS. Compared to Fig. 8, one can clearly conclude that the extended TDNS approach performs much better.

C. Subharmonic Transition at $M_\infty = 4.5$

The flow parameters used in the computations are identical to those in the oblique wave breakdown. A two-dimensional

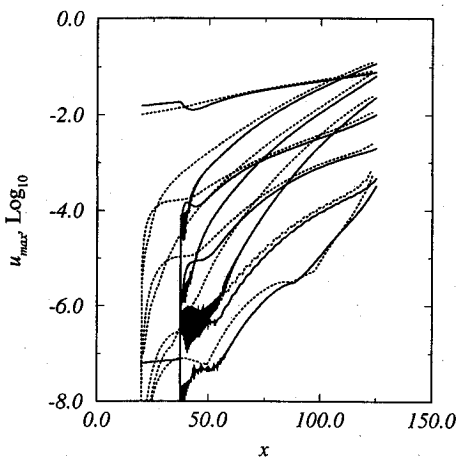

Fig. 9 Comparison between the two different SDNS codes: ——, window approach and ·····, FD approach.

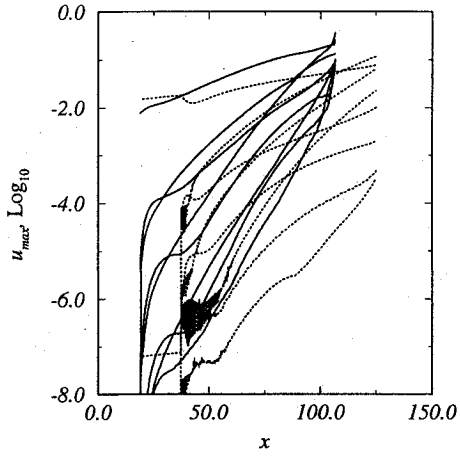

Fig. 10 Comparison between standard TDNS and SDNS: ——, standard TDNS and ·····, SDNS.

second-mode wave with finite amplitude was used to disturb the basic flow, and a pair of oblique waves were used to trigger the onset of the secondary instability. The development of the secondary instability results in the rapid growth of the subharmonic waves, which lead to transition. Both the two- and three-dimensional waves are obtained from LST.[28] In the SDNS, the finite difference approach is used. The amplitude of the second-mode wave, mode (2, 0), is $A_{2D} = 4\%$, and its frequency is $\omega = 2.295$. The oblique waves have the spanwise wave numbers $\beta = 2.1$, and amplitudes $A_{3D} = 0.8\%$. The computational grid is $1150 \times 8 \times 100$ (24 points per wavelength in the x direction). In the computation of the extended TDNS, similar second mode and oblique waves are used as initial disturbances but with amplitudes adjusted to match those in the SDNS. The streamwise wave number of the second mode is $\alpha = 2.52$. The oblique waves have $\alpha = 1.26$. The frame speed is $c_T = 0.82$, which is close to the average group velocity of the second-mode wave. The computational grid is $12 \times 8 \times 140$. Figure 11 shows the streamwise evolution of the leading modes. It can be seen that the agreement between the extended TDNS and SDNS is generally good. The extended TDNS has been able to produce a similar growth pattern to that of the SDNS for all leading modes up to $x = 100$. For $x > 100$, the amplitudes from the SDNS are generally smaller than those from the extended TDNS. This may be partially because of the insufficient resolution in the SDNS in the range $x > 100$. Our other computations with the extended TDNS indicate that mode (0, 4) has reached a significant level at $x = 110$. This mode is not resolved in the computation of the SDNS. Nevertheless, the agreement between the two approaches is considered to be good. Note that in this example the usage of memory and CPU time in the extended TDNS is at least 10 times smaller than that of the SDNS.

Figure 12 shows the comparison between the standard TDNS and SDNS. In the TDNS, the amplitude of the primary oblique waves

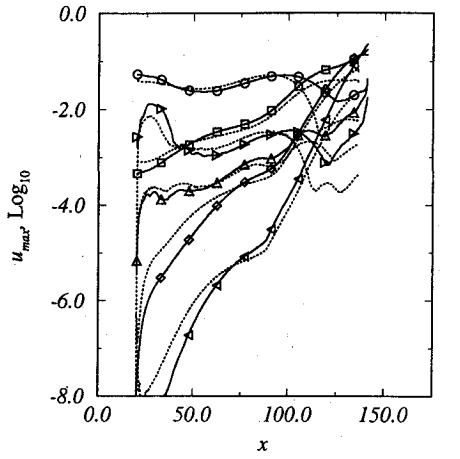

Fig. 11 Maxima of the amplitude functions of the leading modes in a subharmonic transition at $M_\infty = 4.5$, obtained by the extended TDNS and SDNS, finite difference approach: ○, (2, 0); □, (1, 1); ◇, (0, 2); △, (3, 1); ◁, (1, 3); ▷, (4, 0); and ···, SDNS.

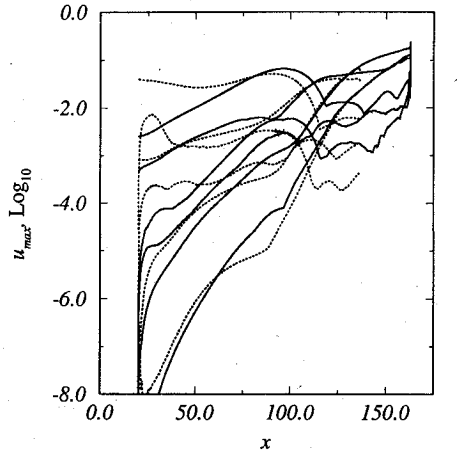

Fig. 12 Comparison between the standard TDNS and SDNS for the subharmonic transition case in Fig. 11: ——, standard TDNS and ·····, SDNS.

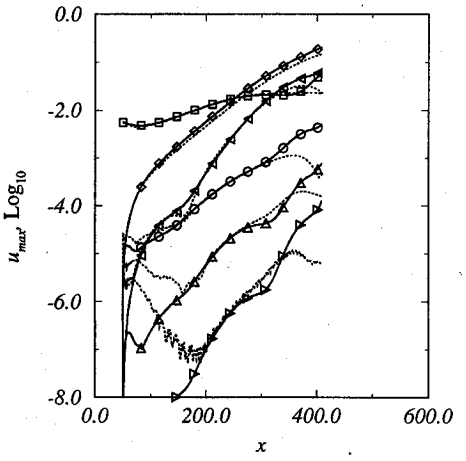

Fig. 13 Oblique wave breakdown at $M_\infty = 1.6$; maxima of the amplitude functions of the leading modes on a logarithmic scale obtained by the extended TDNS and SDNS, finite difference approach: ○, (2, 0); □, (1, 1); ◇, (0, 2); △, (3, 1); ◁, (1, 3); ▷, (4, 0); and ···, SDNS.

is adjusted in such a way that the amplitudes of the leading modes at $x = 110$ match those of the SDNS. Again, we observe a quite different growth pattern from the standard TDNS approach.

D. Oblique Wave Breakdown at $M_\infty = 1.6$

The parameters in this case are chosen to be close to those of Thumm et al.[6]: $M_\infty = 1.6$, $T_\infty = 220$ K, and $Pr = 0.71$. The reference Reynolds number is chosen to be $Re = 2500$ in our

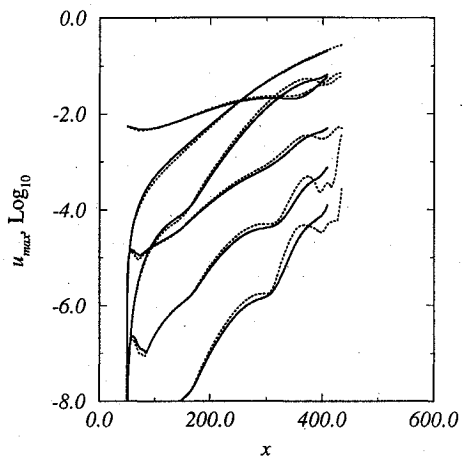

Fig. 14 Comparison between the standard and extended TDNS for the oblique wave breakdown case in Fig. 13: ——, extended TDNS and ·····, standard TDNS.

computations. The flow is initially disturbed by a pair of oblique waves with $\omega = 0.125$ and $\beta = 0.265$. In the computation of the extended TDNS, the streamwise wave number is chosen to be $\alpha = 0.265$, and the frame speed is $c_T = 0.56$. The resolution is $12 \times 12 \times 120$. In the spatial simulation, the finite difference approach is used and the resolution is 36 points per wavelength in the x direction, 8 points in the y direction, and 121 in the z direction. Figure 13 shows the evolution of the maxima of the leading modes. The results from the extended TDNS agree very well with those of the SDNS. In comparison, Fig. 14 shows the results from the standard TDNS approach. Here, only a small difference between the standard TDNS and extended TDNS is observed. At this low Mach number, both approaches give satisfactory results.

V. Discussion and Concluding Remarks

A quantitative comparison study between temporal and spatial DNS has been performed. This study shows that our extended TDNS approach is able to produce simulation results comparable with those of SDNS at high Mach numbers, where the standard TDNS approach is not satisfactory.

There is of course the basic question of how to compare TDNS results with SDNS results. In this study, the maximum of the amplitude function of a streamwise spatial Fourier mode in a TDNS is compared with that of a temporal Fourier mode in an SDNS. This is rather stringent, since any difference in the flowfield will give a different composition of all leading modes.

One advantage of the extended TDNS is that it allows us to simulate the whole transition process from laminar to turbulent state much more efficiently than an SDNS. In all our computations at low resolution, the extended TDNS requires at least 10 times less memory and CPU time than an SDNS does. At higher resolution, an SDNS will become even more expensive.

Compared to a PSE approach,[35] we have the following comments. A PSE approach is generally more accurate and cheaper than the extended TDNS for the linear and weakly nonlinear stages of transition, but it does not allow one to simulate the transition process deep into the breakdown stage. The extended TDNS, on the other hand, can give us reasonable results for the linear and nonlinear stages and allows us to march through the breakdown stage and to enter the turbulent stage. Thus, the extended TDNS can be viewed as a valuable tool in the sense that it allows us to study a complete transition process on today's supercomputers.

Acknowledgments

Part of this work was supported by the Deutsche Forschungsgemeinschaft. Computations for this work were performed while the first two authors were affiliated with DLR Göttingen in Germany. We are grateful to a referee for his constructive comments on an earlier version of this paper.

References

[1]Pruett, C. D., and Chang, C.-L., "Spatial Direct Numerical Simulation of High-Speed Boundary-Layer Flows—Part II: Transition on a Cone in Mach 8 Flow," *Theoretical Computational Fluid Dynamics*, Vol. 7, No. 5, 1994, pp. 397–424.

[2]Rai, M. M., and Moin, P., "Direct Numerical Simulation of Transition and Turbulence in a Spatially Evolving Boundary Layer," *Journal of Computational Physics*, Vol. 109, 1993, pp. 169–192.

[3]Eißler, W., and Bestek, H., "Spatial Numerical Simulation of Nonlinear Transition Phenomena in Supersonic Boundary Layers," *Transitional and Turbulent Compressible Flows*, edited by L. D. Kral and T. A. Zang, FED-Vol. 151, American Society of Mechanical Engineers, New York, 1993, pp. 69–76.

[4]Fasel, H., Rist, U., and Konzelmann, U., "Numerical Investigation of the Three-Dimensional Development in Boundary-Layer Transition," *AIAA Journal*, Vol. 28, 1990, pp. 29–37.

[5]Pruett, C. D., Zang, T. A., Chang, C.-L., and Carpenter, M. H., "Spatial Direct Numerical Simulation of High-Speed Boundary-Layer Flows—Part I: Algorithmic Considerations and Validation," *Theoretical Computational Fluid Dynamics*, Vol. 7, No. 1, 1994, pp. 49–76.

[6]Thumm, A., Wolz, W., and Fasel, H., "Numerical Simulation of Spatially Growing Three-Dimensional Disturbance Waves in Compressible Boundary Layers," *Laminar-Turbulent Transition*, edited by D. Arnal and R. Michel, Springer–Verlag, Berlin, 1989, pp. 303–308.

[7]Kleiser, L., and Zang, T. A., "Numerical Simulation of Transition in Wall-Bounded Shear Flows," *Annual Review of Fluid Mechanics*, Vol. 23, 1991, pp. 495–537.

[8]Dinavahi, S. P. G., Pruett, C. D., and Zang, T. A., "Direct Numerical Simulation and Data Analysis of a Mach 4.5 Transitional Boundary-Layer Flow," *Physics of Fluids*, Vol. 6, No. 3, 1993, pp. 1323–1330.

[9]Guo, Y., Adams, N. A., Sandham, N. D., and Kleiser, L., "Numerical Simulation of Supersonic Boundary Layer Transition," AGARD-CP-551, Dec. 1994, pp. 13-1–13-12.

[10]Adams, N. A., "Numerische Simulation von Transitionsmechanismen in kompressiblen Grenzschichten," Ph.D. Dissertation, Dept. of Mechanical Engineering, Technical Univ. of Munich, Germany, July 1993; also DLR-FB 93-29, DLR, German Aerospace Research Establishment.

[11]Adams, N. A., and Kleiser, L., "Numerical Simulation of Fundamental Breakdown of a Laminar Boundary-Layer at Mach 4.5," AIAA Paper 93-5027, Dec. 1993.

[12]Adams, N. A., and Kleiser, L., "Subharmonic Transition to Turbulence in a Flat Plate Boundary Layer at Mach Number 4.5," *Journal of Fluid Mechanics* (submitted for publication).

[13]Ducros, F., Comte, P., and Lesieur, M., "Ropes and Lambda-Vortices in Direct and Large-Eddy Simulation of a High-Mach Number Boundary Layer over a Flat Plate," 9th Symposium on Turbulent Shear Flow, Kyoto, Japan, 1993.

[14]Erlebacher, G., and Hussaini, M. Y., "Numerical Experiments in Supersonic Boundary Layer Stability," *Physics of Fluids A*, Vol. 2, 1990, pp. 94–104.

[15]Pruett, C. D., and Zang, T. A., "Direct Numerical Simulation of Laminar Breakdown in High-Speed, Axisymmetric Boundary Layers," *Theoretical Computational Fluid Dynamics*, Vol. 3, No. 6, 1992, pp. 345–367.

[16]Sandham, N. D., Adams, N. A., and Kleiser, L., "Direct Simulation of Breakdown to Turbulence Following Oblique Instability Waves in a Supersonic Boundary Layer," *Direct and Large-Eddy Simulation I*, edited by P. R. Voke, L. Kleiser, and J. P. Chollet, 1994, Kluwer, London, pp. 213–223.

[17]Spalart, P. R., and Yang, K. S., "Numerical Study of Ribbon-Induced Transition in Blasius Flow," *Journal of Fluid Mechanics*, Vol. 178, 1987, pp. 345–365.

[18]Bertolotti, F. P., Herbert, T., and Spalart, P. R., "Linear and Nonlinear Stability of the Blasius Boundary Layer," *Journal of Fluid Mechanics*, Vol. 242, 1992, pp. 441–471.

[19]Guo, Y., Adams, N. A., and Kleiser, L., "Modeling of Nonparallel Effects in Temporal DNS of Compressible Boundary Layer Transition," *Theoretical Computational Fluid Dynamics*, Vol. 7, No. 2, 1994, pp. 141–157.

[20]Lin, C. C., *Theory of Hydrodynamic Stability*, Cambridge Univ. Press, New York, 1955.

[21]Guo, Y., and Adams, N. A., "A Spectral/Finite-Difference Algorithm for Direct Numerical Simulation of Spatially Evolving Compressible Boundary Layer Transition," Internal Rept. DLR-IB 221-93 A 26, DLR, Inst. for Fluid Mechanics, Göttingen, Germany, 1993.

[22]Guo, Y., Adams, N. A., and Kleiser, L., "Direct Numerical Simulation of Transition in a Spatially Growing Compressible Boundary Layer Using a New Fourier Method," *Direct and Large-Eddy Simulation I*, edited by P. R. Voke, L. Kleiser, and J. P. Chollet, 1994, Kluwer, London, pp. 249–259.

[23]Poinsot, T. J., and Lele, S. K., "Boundary Condition for Direct Simulation of Compressible Viscous Flow," *Journal of Computational Physics*, Vol. 101, 1992, pp. 104–129.

[24]Pruett, C. D., and Chang, C.-L., "A Comparison of PSE and DNS for High-Speed Boundary-Layer Flows," *Transitional and Turbulent Compressible Flows*, edited by L. D. Kral and T. A. Zang, FED-Vol. 151, American Society of Mechanical Engineering, New York, 1993, pp. 57–67.

[25]Spalart, P. R., "Direct Numerical Study of Leading-Edge Contamination," *Fluid Dynamics of Three-Dimensional Turbulent Shear Flows and Transition*, AGARD-CP-438, 1989, pp. 5.1–5.13.

[26]Givoli, D., "Non-Reflecting Boundary Conditions," *Journal of Computational Physics*, Vol. 94, 1991, pp. 1–29.

[27]Israeli, M., and Orszag, S. A., "Approximation of Radiation Boundary Conditions," *Journal of Computational Physics*, Vol. 41, 1981, pp. 115–135.

[28]Simen, M., "COSMET, a DLR-Dornier Program for Compressible Stability Analysis with Local Metric," Internal Rept. IB 221-91 A 09, DLR, Inst. for Theoretical Fluid Mechanics, Göttingen, Germany, 1991.

[29]Mack, L. M., "Boundary-Layer Linear Stability Theory," Special Course on Stability and Transition of Laminar Flow, AGARD Rept. 709, 1984, pp. 3.1–3.81.

[30]Joslin, R. D., Streett, C. L., and Chang, C.-L., "Validation of Three-Dimensional Incompressible Spatial Direct Numerical Simulation Code," NASA TP 3205, 1992.

[31]Liu, C., and Liu, Z., "High Order Finite Difference and Multigrid Methods for Spatially Evolving Instability in a Planar Channel," *Journal of Computational Physics*, Vol. 106, 1993, pp. 92–100.

[32]Guo Y., "An Analysis of Repetitive Signal by Cepstrum," *Journal of Beijing University of Science and Technology*, Vol. 9, 1987, pp. 48–56.

[33]Harris, F. J., "On the Use of Windows for Harmonic Analysis with the Discrete Fourier Transform," *Proceedings of the IEEE*, Vol. 66, 1978, pp. 51–83.

[34]Guo, Y., and Adams, N. A., "A Numerical Investigation of Supersonic Turbulent Boundary Layers with High Wall Temperature," *Proceedings of the Summer Program 1994*, Center for Turbulence Research, Stanford Univ./NASA Ames Research Center, 1994, pp. 245–267.

[35]Bertolotti, F. P., "Compressible Boundary Layer Stability Analyzed with the PSE Equations," AIAA Paper 91-1637, 1991.